"Augmented Reality" in Conventional Simulation by Projection of 3-D Structures into 2-D Images

A Comparison with Virtual Methods

Heinz Deutschmann[1,2], Philipp Steininger[2,3], Olaf Nairz[1,2], Peter Kopp[1], Florian Merz[1], Karl Wurstbauer[1], Franz Zehentmayr[1,2], Gerd Fastner[1,2], Manfred Kranzinger[1], Gerhard Kametriser[1], Michael Kopp[1], Felix Sedlmayer[1,2]

Background and Purpose: In this study, a new method is introduced, which allows the overlay of three-dimensional structures, that have been delineated on transverse slices, onto the fluoroscopy from conventional simulators in real time.
Patients and Methods: Setup deviations between volumetric imaging and simulation were visualized, measured and corrected for 701 patient isocenters.
Results: Comparing the accuracy to mere virtual simulation lacking additional X-ray imaging, a clear benefit of the new method could be shown. On average, virtual prostate simulations had to be corrected by 0.48 cm (standard deviation [SD] 0.38), and those of the breast by 0.67 cm (SD 0.66).
Conclusion: The presented method provides an easy way to determine entity-specific safety margins related to patient setup errors upon registration of bony anatomy (prostate 0.9 cm for 90% of cases, breast 1.3 cm). The important role of planar X-ray imaging was clearly demonstrated. The innovation can also be applied to adaptive image-guided radiotherapy (IGRT) protocols.

Key Words: Conventional simulation · Virtual simulation · Augmented reality · IGRT · Safety margins

Strahlenther Onkol 2008;184:93–9
DOI 10.1007/s00066-008-1742-5

Unterstützung der konventionellen Simulation in der Strahlentherapie durch Einblendung von dreidimensionalen Strukturen. Vergleich mit virtuellen Methoden

Hintergrund und Ziel: Es wird ein Verfahren vorgestellt, das die Einblendung von dreidimensionalen Strukturen, die zuvor z.B. auf axialen Schnittbildern segmentiert wurden, in Durchleuchtungsaufnahmen am konventionellen Simulator in Echtzeit erlaubt.
Patienten und Methodik: Mit dieser Technologie wurden an 701 Patientenisozentren Lagerungsunterschiede zwischen der Schnittbildgebung und der Simulation visualisiert, vermessen und korrigiert.
Ergebnisse: Im Vergleich der Genauigkeit mit der rein virtuellen Simulation, bei der auf Röntgenbildgebung verzichtet wird, zeigte sich eine deutliche Überlegenheit der neuen Methode. Im Mittel wurden virtuell simulierte Prostatabestrahlungen um 0,48 cm (Standardabweichung [SD] 0,38) und jene der Mamma um 0,67 cm (SD 0,66) korrigiert.
Schlussfolgerung: Das vorgestellte Verfahren erlaubt die einfache Bestimmung entitätsspezifischer Sicherheitsränder für Lagerungsungenauigkeiten von knöchernen Strukturen (Prostatabestrahlung 0,9 cm für 90% der Fälle, Mamma 1,3 cm; Tabelle 2). Die Bedeutung von planarer kV-Bildgebung konnte gezeigt werden. Das innovative Verfahren ist auch im Rahmen von Protokollen zur adaptiven, bildgeführten Radiotherapie (IGRT) einsetzbar.

Schlüsselwörter: Konventionelle Simulation · Virtuelle Simulation · Augmented Reality · IGRT · Sicherheitsränder

[1] University Clinic for Radiotherapy and Radio-Oncology, Salzburg, Austria,
[2] radART – Institute for research and development on Advanced Radiation Technologies at the Paracelsus Medical University, Salzburg, Austria,
[3] Department of Medical Computer Science and Technology, University for Health Sciences, Hall i. T., Austria.

Received: April 30, 2007; accepted: December 13, 2007

Introduction

In radiotherapy, simulation is an established tool for field arrangement or transfer of previously planned beams. For delineation of relevant field settings on the patient, the use of special dye application can facilitate setup reproducibility [23].

Conventional simulators are supporting this process by X-ray imaging [6]. With the help of fluoroscopy – in simple cases – the field size or the angle of entry can be determined in a "beam's eye view" perspective and ports can directly be marked with the help of lightfield projections. More complex treatment plans can be adjusted by comparing X-ray images with digitally reconstructed radiographs (DRRs) [17] derived from volume datasets [10]. Using conventional simulation, online images are obtained and variations in positioning of the patient can be checked immediately. The process can be supplemented by application of contrast agents and allows examination of organ movements (see Figure 3). Based upon fine detailed X-ray images, field modifications as well as exact definitions of blocks are possible.

Virtual simulation [14] works exclusively with a digital 3-D representation of the patient: isocenters are defined upon slices whilst irregular field boundaries are usually determined using computer-generated visualization of structure sets, i.e., the surface of the target volume and the organs at risk. The coordinates of field entry points and isocenters thus defined can be projected and marked onto the patient's skin with maneuverable laser systems.

Meanwhile, CT-based and highly conformal techniques with precisely reproducible positioning have become state of the art in radiotherapy [16], allowing to spare normal tissue and to reduce safety margins [9–11]. Primary conventional simulation has lost importance, as actual imaging of the virtually simulated patient is frequently postponed and performed within the first treatment session followed by assessment of verification images [2, 21].

The aim of this study was to analyze differences in precision of virtual simulation and advanced conventional simulation enhanced by 3-D overlays – as to our knowledge introduced for the first time.

Patients and Methods

The term *augmented virtuality* (AV) originates from multimedia computer animations, referring to the opportunity of embedding real events in a virtual surrounding. *Augmented reality* (AR) denotes the process of overlaying virtual, computer-generated structures on "real" images – e.g., a 3-D structure overlay on X-ray images from the simulator [13].

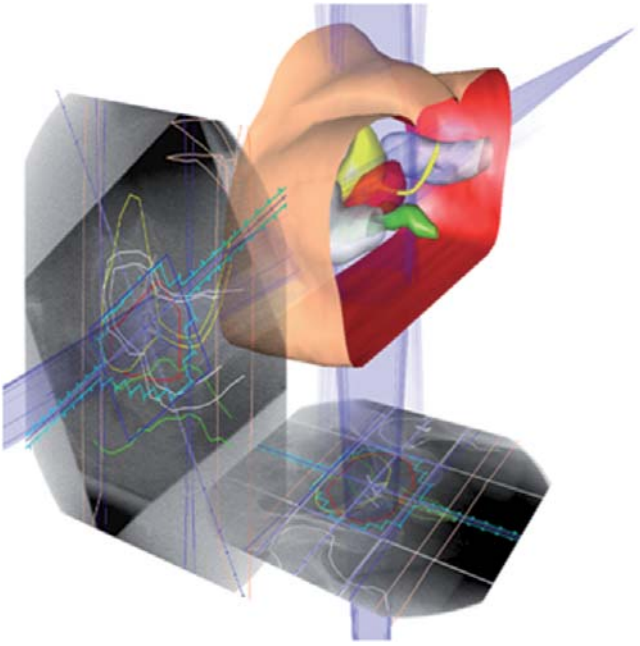

Figure 1. Projection of 3-D structures into the image plane: the principle of registration by assignment of the image to a field, quotation of the SFD and the 2-D position of the central axis in the image.

Abbildung 1. Projektion der 3-D-Strukturen in die Bildebene: Prinzip der Registrierung durch Zuordnung der Aufnahme zu einem Feld, Angabe des Fokus-Film-Abstands und der 2-D-Position des Zentralstrahls im Bild.

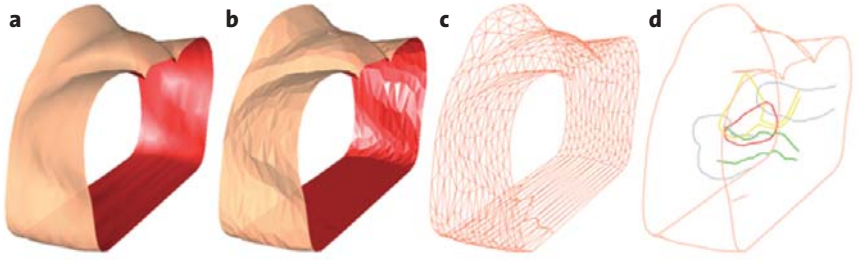

Figures 2a to 2d. Depiction of structured surfaces: 12-mm scan of the body surface, compiled by contoured polygons with 8 mm space between slices. a) Smoothing of the image by processing the surface normal of each vertex. b) Faceted depiction by processing of only one surface normal per triangle. c) Triangulation of the contour polygons – 1,026 lines (2-D) build up 1,910 triangles with a total of 2,936 edges (3-D). d) Reduction of the image resulting in an "artificial sketch" – shadow depiction of a radiopaque structure. The number of lines for the body surface could – in this projection with profile display – be reduced to 146 (including the lowermost and topmost contour from 288, here), among those 36 (66) part of the silhouette.

Abbildungen 2a bis 2d. Darstellung von Strukturoberflächen: 12 cm langer Scan der Körperoberfläche, aufgebaut aus Konturpolygonen mit 8 mm Schichtabstand. a) Glättung der Darstellung durch Berechnung der Oberflächennormalen für jeden Punkt. b) Facettierte Darstellung durch Berechnung von nur einer Oberflächennormale je Dreieck. c) Triangulation der Konturpolygone – 1026 Streckenzüge (2-D) bauen 1910 Dreiecke mit insgesamt 2936 Kanten (3-D) auf. d) Reduktion zu einem „artificial sketch" – Schattendarstellung von radiopaken Strukturen. Für die Körperoberfläche konnte die Linienzahl in dieser Projektion in Profildarstellung auf 146 (inklusive unterster und oberster Kontur auf hier dargestellte 288), davon Teil der Silhouette 36 (66), reduziert werden.

We developed a system, which enables an overlay of inner structures, target volumes and organs at risk as well as field boundaries; these can be imported from treatment-planning systems via DICOM and projected onto the X-ray plane in real time – i.e., while a fluoroscopy is performed [3]. The software with the provisional name *rt² visual control* (*rt²* = real-time radiotherapy) permits the simultaneous display of *virtual* material (e.g., a projection of 3-D structures that might not have been visible in the fluoroscopy due to missing soft-tissue contrast) and *real* material (the current X-ray image) on one canvas. The assignment of the two realities is performed semiautomatically by utilization of the same system of coordinates as defined by the DICOM frame of reference, in which geometric field data such as the position of the isocenter and the gantry angle as well as the structure points are defined. If the distance between source and film (SFD) is known and the position and orientation of the central axis in the X-ray image (2-D) is given, the picture can be brought into a 3-D, unambiguous relation with the virtual patient, provided it is linked to a geometrically defined beam (see Figures 1 and 2).

For this purpose, technically, the analog video signal from the simulator's image intensifier chain (Oldelft Simulix) is digitized on a frame grabber card (HaSoTec FG-3x) within a standard PC with a frame rate of 25 Hz at 768 × 576 pixels in a grayscale resolution of 8 bit. These preliminary images show a cushion-shaped distortion, which is corrected automatically before registration. The software works as a client server application and allows immediate, full access to all radiotherapy-relevant patient data due to its bidirectional interfaces to treatment-planning systems, imaging modalities (CT, MRI, PET) and linear accelerators.

For example, structure data transmitted as a DICOM RT Structure Set are organized as a sequence of points in contour polygons which have been drawn on CT slices [4, 19]. A coordinate transformation can be applied to the single points on the surface, bringing them into the coordinate system of the field that is, among others, defined by the central axis focus – isocenter. The projection of the individual points from the structure surface to the image plane can then easily be achieved by applying the theorem of intercepting lines.

Augmented Simulation

In order to compare the precision of the 3-D-supported conventional simulation introduced here with the method of virtual simulation, 701 patient isocenters in different entities (see Table 1) were simulated between 07/2004 and 07/2006,

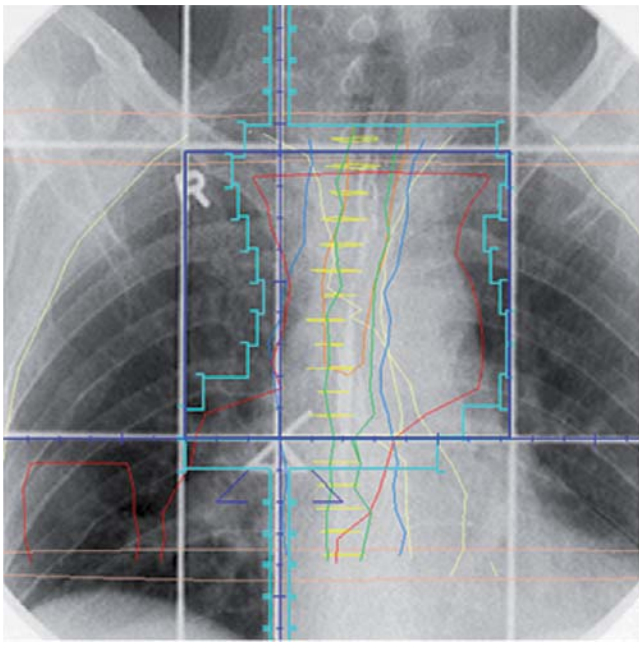

Figure 3. Simulation of a lung field: the contrast agent is visible within the esophagus; the dynamic process can be observed in the X-ray between the outline of the projected 3-D structure (green).

Abbildung 3. Simulation einer Lungenbestrahlung: Dargestellt ist die Kontrastmittelgabe im Ösophagus; die Schluckbewegung kann im Röntgenbild zwischen dem Linienschatten der projizierten 3-D-Struktur (grün) verfolgt werden.

each simulation starting from an initial point of reference. This point of reference was visualized in the CT with three marker wires (left, right, anterior/posterior) on the skin of

Table 1. Distribution of deviations within registration of bony structures, esophagus, trachea, lungs and list of most common deviations (standard deviations [SD] in parenthesis). A-P: anterior-posterior; C-C: cranio-caudal; L-R: left-right.

Tabelle 1. Verteilung der Abweichungen bei Registrierung auf knöcherne Strukturen, Ösophagus, Trachea, Lunge sowie Darstellung der häufigsten Abweichungen (in Klammern sind die Standardabweichungen [SD] angegeben). A-P: anterior-posterior; C-C: kranio-kaudal; L-R: links-rechts.

Entity	Isocenters (n)	Mean error (± SD; cm) L-R	A-P	C-C	Vector V
Prostate	158	0.07 (± 0.36)	−0.06 (± 0.43)	0.01 (± 0.24)	0.48 (± 0.38)
Bladder	16	0.00 (± 0.39)	0.12 (± 0.32)	0.09 (± 0.25)	0.50 (± 0.30)
Rectum	35	−0.03 (± 0.49)	0.06 (± 0.49)	0.08 (± 0.45)	0.62 (± 0.56)
Gynecologic	37	0.26 (± 0.53)	0.18 (± 0.54)	0.09 (± 0.39)	0.67 (± 0.62)
Abdomen	12	−0.01 (± 0.30)	0.15 (± 0.32)	0.14 (± 0.44)	0.45 (± 0.47)
Thorax	74	−0.06 (± 0.23)	0.00 (± 0.47)	0.03 (± 0.39)	0.44 (± 0.48)
Mamma	332	0.02 (± 0.54)	0.10 (± 0.65)	0.07 (± 0.37)	0.67 (± 0.66)
Head and neck	17	0.08 (± 0.38)	−0.34 (± 0.53)	0.07 (± 0.19)	0.58 (± 0.50)
Skull	10	0.00 (± 0.10)	−0.03 (± 0.27)	−0.01 (± 0.14)	0.26 (± 0.19)
Other	10	0.01 (± 0.33)	0.21 (± 0.21)	0.56 (± 1.43)	0.91 (± 1.32)
Total	701	0.03 (± 0.46)	0.05 (± 0.56)	0.06 (± 0.39)	0.59 (± 0.59)

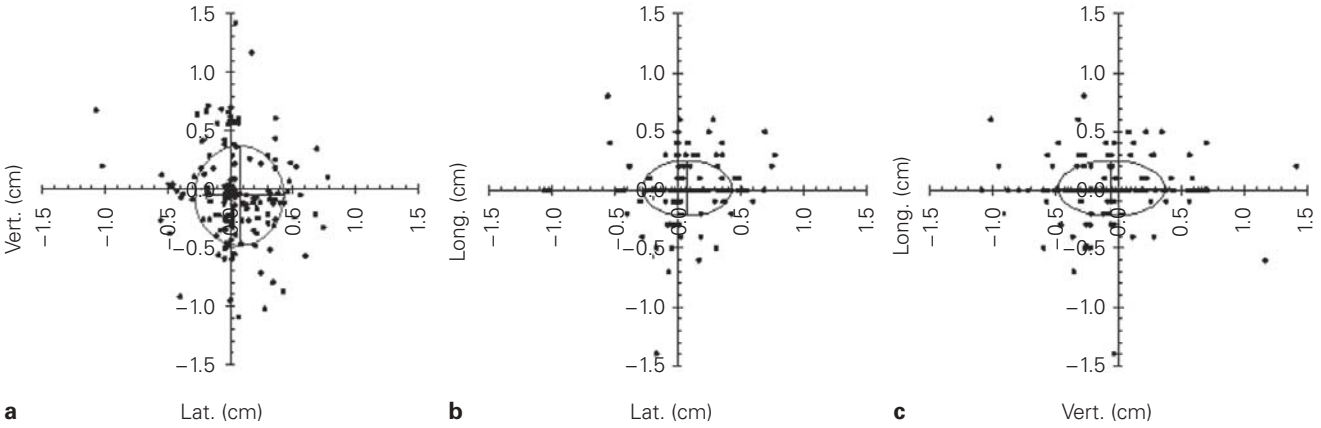

Figures 4a to 4c. n. prostatae (n = 158): scatter of deviations between virtual simulation and conventional simulation, supported by an overlay of inner structures (os pubis, femoral heads), which had been segmented in CT slices. a) Transverse image (A-P vs. L-R). b) Coronal image (C-C vs. L-R). c) Sagittal image (A-P vs. C-C). The ellipses mark the area of one standard deviation, the point of intersection of the main axis marks the mean of the scatter.

Abbildungen 4a bis 4c. n. prostatae (n = 158): Streuung der Abweichungen zwischen virtueller Simulation und konventioneller Simulation, unterstützt durch Einblendung von inneren Strukturen (Os pubis, Femurköpfe), die zuvor auf Schnittbildern (CT) segmentiert wurden. a) Transversale Darstellung (A-P vs. L-R). b) Koronale Darstellung (C-C vs. L-R). c) Sagittale Darstellung (A-P vs. C-C). Die eingezeichneten Ellipsen markieren das Gebiet der einfachen Standardabweichung, der Schnittpunkt der Hauptachsen gibt den Mittelwert der Streuung an.

the patients. Following the rules of virtual simulation, the conventional simulator's bench was moved in x/y/z direction according to the distance from the point of reference to the isocenter: without further imaging, the elaborated position can be considered the respective isocenter and the latter could have been marked on the patient's skin – as a result of the virtual simulation. Following an X-ray, taken in this very position, the immediate fusion with 3-D structures that were visible upon the image (e.g., bones, the trachea, the esophagus with a contrast medium, lungs, skin) was performed. Deviations between the image of the overlaid "virtual" structures and the "real" structures as seen in the fluoroscopy were measured by moving the couch along three axes Δx, Δy, Δz. The value and the direction of the absolute shift vector $\vec{V}$, which marks the difference between the two methods, were computed according to equation 1 and kept as a record:

$$V = \sqrt{\Delta x^2 + \Delta y^2 + \Delta z^2} \qquad \text{(equation 1)}.$$

The marks on the patient's skin were drawn following a position adjustment that was performed according to the optimum correspondence of the projected lines and the structures visible in the X-ray.

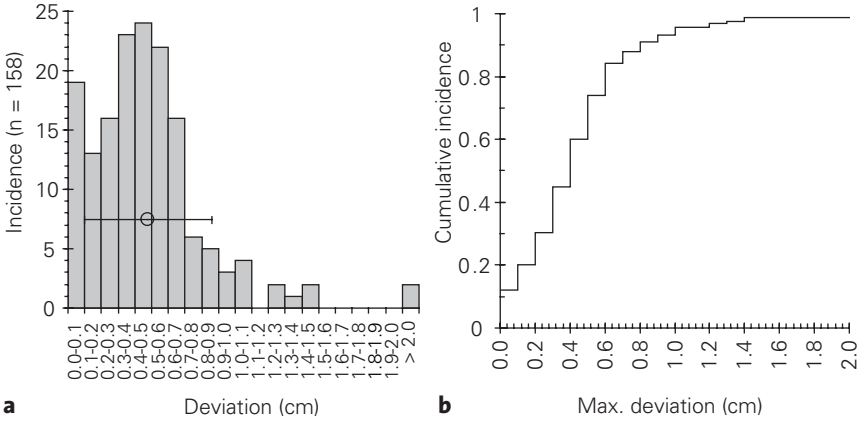

Figures 5a and 5b. n. prostatae: distribution of deviations. a) Histogram with mean error and SD. b) Cumulative graph, standardized.

Abbildungen 5a und 5b. n. prostatae: Verteilung der Abweichungen. a) Histogramm mit mittlerem Fehler und Standardabweichung. b) Kumulative Darstellung, normiert.

Results

Systematic errors in the virtual simulation were not detected (< 1 mm) – on average, the positions of the isocenters gained by 3-D-supported conventional simulation were the same. However, a significant scatter around zero with mean errors that varied according to the respective entity, could be shown (see Figures 4 and 6, and Figure 8, Table 1). On the whole, these deviations can be explained by divergent positioning or tenseness of the patient on the CT bench and on the simulation couch and by internal organ motions: the positions for head treatment (where the head had been fixated with thermoplastic masks) could be reproduced more precisely with

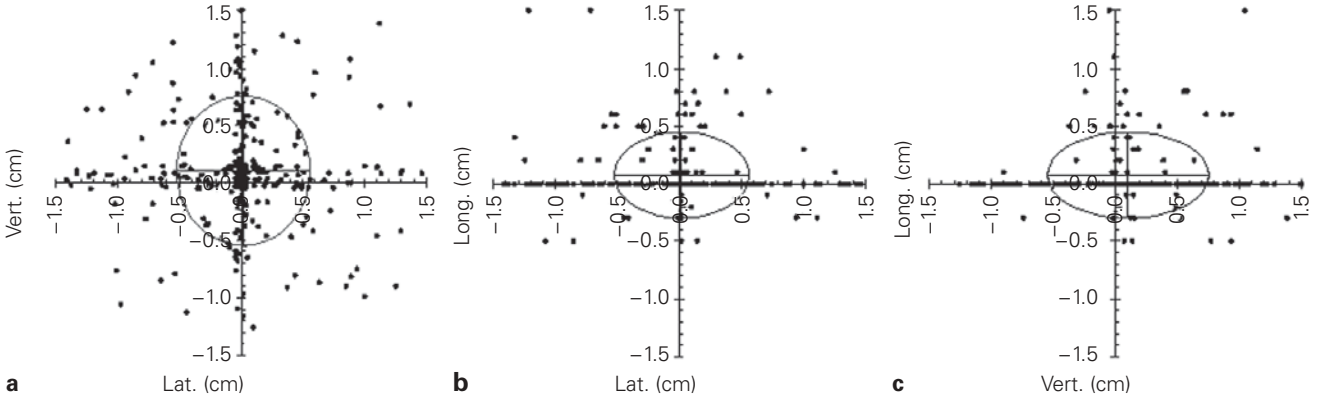

Figures 6a to 6c. n. mammae (n = 332 isocenters): scatter of deviations when structures (body surface, lungs) are faded into the image (cf. Figure 4).

Abbildungen 6a bis 6c. n. mammae (n = 332 Isozentren): Streuung der Abweichungen bei Einblendung von Strukturen (Körperoberfläche, Lungen) (vgl. Abbildung 4).

a mean of 2.6 mm (standard deviation [SD] 1.9) than for treatment of the pelvic area (where the patient is either in the prone position supported by a belly board or in the supine position with a knee cushion) with a mean of 4.6 mm (SD 5.3). Naturally, the positions for breast treatment (with wedges, armrests) were most difficult to be reproduced, showing means of 6.6 mm (SD 6.7).

The histogram of the error distribution shows an entity-specific quantitative interaction between the reproducibility of the positions and the safety margins required for a statistical probability of hits with regard to the respective internal structures concerned (see Figures 5 and 7, Table 2). The analysis of pelvic treatment accuracy shows that the required safety margins for 90% hits (registration upon bony anatomy) seem to be significantly smaller for the supine position with 8 mm (bladder, prostate) than for the prone position with 12 mm (rectum, gynecologic indications) [12].

Discussion

The scatter of the detected deviations in the C-C (cranio-caudal) direction is smaller in all entities than the ones detected for the left-right (L-R) and the anterior-posterior (A-P) direction. This may be traced back mainly to the considerable distance between the underlying CT slices (3–10 mm) resulting in unsatisfactory detail resolution of the reconstructed surfaces in this direction.

Tilts were not considered separately in this study, even though our software supports all rigid transformations of structure sets, including rotations [15]. These can be neglected as those rotations, which appear to be most significant in radiotherapy, refer to internal organ movements: the prostate is rotating up to 30° around the L-R axis through the apex caused by varying filling of the rectum and the bladder [5, 7, 8]. Such movements cannot be visualized without radiopaque marker seeds in X-rays. The usual tilts of the whole pelvis appear to be secondary in this respect.

The safety margins provided (Table 2) refer exclusively to the probability of hits relating to visible "internal fiducials" (in the pelvis: bony structures); they therefore have to be enlarged corresponding to the inner movement of the target volumes and by additional margins accounting for delineation errors, if a planning target volumen is derived from a clinical target volume [20, 22].

For the individual patient the comparably high translatory deviations from virtual simulation to 3-D-supported conventional simulation would have led to severe errors in radiotherapy, if the erroneous results from the virtual simulation had been perpetuated by marking the patient's skin.

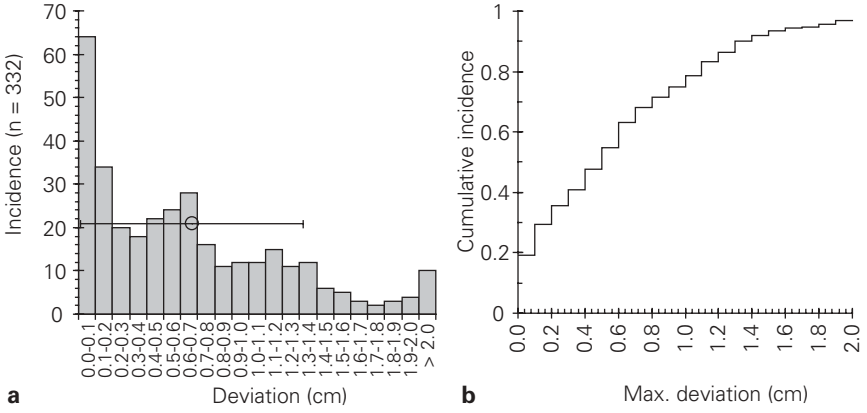

Figures 7a and 7b. n. mammae: distribution of deviations. a) Histogram with mean error and SD. b) Cumulative graph, standardized.

Abbildungen 7a und 7b. n. mammae: Verteilung der Abweichungen. a) Histogramm mit mittlerem Fehler und Standardabweichung. b) Kumulative Darstellung, normiert.

Patients whose isocenters were determined by virtual simulation require a confirmation of the skin marking in any case. However, this can be performed during the first treatment session at the linac, either by a suitable MV imaging technique (e.g., field-in-field images) or preferably by planar or volumetric kV imaging during image-guided radiotherapy (IGRT). Figure 9 shows an application of the presented fusion method in this field: due to the rigid alignment of the X-ray tube and an amorphous silicon flatpanel detector mounted on a linac, the X-ray images can be registered after performing a flex-map correction, which considers the replicable mechanical stability of tube, panel and isocenter all-automatically. The output image can then be fused immediately at the start of the recording, and a reference image (e.g., DRR) can be overlaid directly. This opens further potentials in the context of IGRT for the technology introduced and may contribute to a reduction of time-consuming and dose-intensive volume data acquisitions – cone-beam reconstructions – by applying the much faster, planar imaging technique and 2-D-3-D registration. The role of conventional X-ray images for the accuracy of treatment is to be reevaluated in this respect.

Table 2. Analysis of cumulative distribution of errors; isotropic safety margins relate to hit rate upon registration of structures visible in X-ray (bones, air cavities, contrast media).

Tabelle 2. Auswertung der kumulativen Fehlerverteilung; isotrope Sicherheitsränder beziehen sich auf Treffsicherheit bei Registrierung auf Strukturen, die im Röntgenbild sichtbar sind (Knochen, Lufträume, Kontrastmittel, Haut).

Entity	Isocenters (n)	Required safety margin for hit rate (cm)			
		50%	80%	90%	95%
Prostate	158	0.4	0.6	0.9	1.0
Bladder	16	0.3	0.7	0.9	1.1
Rectum	35	0.4	0.7	1.2	> 2.0
Gynecologic	37	0.4	0.8	1.6	1.6
Abdomen	12	0.2	0.6	1.0	1.6
Thorax	74	0.3	0.7	0.9	1.2
Mamma	332	0.5	1.1	1.3	1.7
Head and neck	17	0.4	1.0	1.5	1.7
Skull	10	0.2	0.4	0.4	0.6
Pelvis supine	174	0.4	0.6	0.8	1.1
Pelvis prone	72	0.4	0.8	1.2	1.8

Conclusion

Due to organ movement, skin markings are less reliable than "internal fiducials". Bones and other landmark structures such as trachea, esophagus or marker seeds that can be implanted in the target area, show little to no relative movements toward the target volume. The presented method provides an uncomplicated way of adjusting rays precisely to such inner structures. 3-D-supported fluoroscopy enables significantly

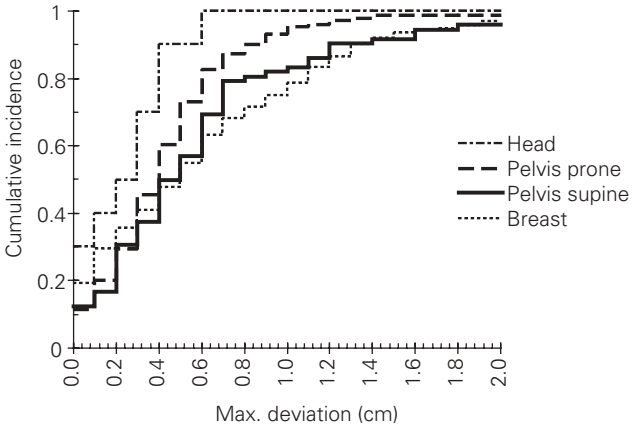

Figure 8. Comparison of reproducibility of positions for radiotherapy of the head with fixation mask, the pelvis in supine/prone position and the mamma.

Abbildung 8. Gegenüberstellung der Reproduzierbarkeit von Lagerungen für Bestrahlungen im Schädel mit Maskenfixation, im Becken bei Rücken- bzw. Bauchlage und der Mamma.

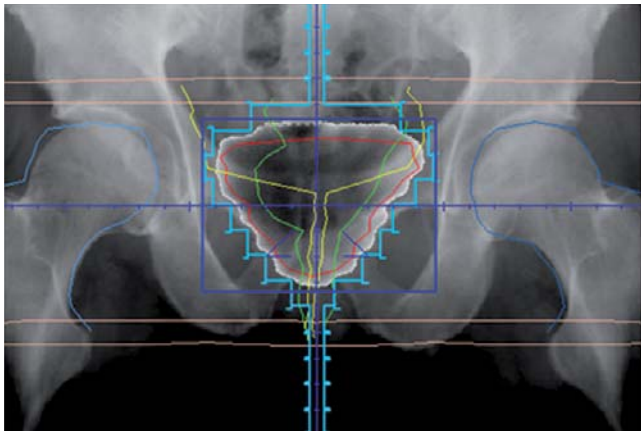

Figure 9. IGRT: ventral images of the pelvis – kV image from the onboard X-ray unit of a linac, which has been registered all-automatically and has been overlaid with the respective MV verification image and the projections of inner structures from a CT scan. The evaluation of accuracy of the position as well as that of field boundaries is possible in the fusion image.

Abbildung 9. IGRT: ventrale Beckenaufnahmen – kV-Aufnahme der Röntgeneinheit am Linearbeschleuniger, die vollautomatisch registriert und mit der zugehörigen MV-Verifikationsaufnahme sowie den Projektionen der inneren Strukturen aus der CT überlagert wurde. Die Überprüfung von Lagerungsgenauigkeiten und Feldbegrenzungen ist im Fusionsbild bei geeigneter Fensterung möglich.

more precise markings of isocenters than virtual simulation, if there are significant time gaps or repositionings between tomography and the skin marking process. The method of 3-D-supported conventional simulation is simple, usability is intuitive, and image quality is superior to DRRs. In case of deviations between the "real" and the "virtual" patient, the physician may perform and control corrections instantly with imaging feedback in real time. As predetermined field boundaries (blocks, multileaf collimators) can be faded into the image (or drawn/modified), an immediate and exact control of these machine parameters is facilitated by comparing the field boundaries of the planned beam with verification portal images. Quantitative analysis of setup accuracy and determination of implied safety margins can be performed.

A fast way to easily track rotations on planar images is still to be found [18]. A corresponding study that involves the use of radiopaque marker seeds [1] that can, for example, be implanted into the prostate and then be traced online via planar-view IGRT, is currently undergoing a prospective trial at our department.

Acknowledgment

This study has been partly supported by Elekta within the scope of a research collaboration at radART – Institute for research and development on Advanced Radiation Technologies at the Paracelsus Medical University, Salzburg.

References

1. Beltran C, Herman M. Intra-fraction prostate motion and margin calculations for prostate radiotherapy using electronic portal imaging, implanted fiducials and four localization methods. Med Phys 2006;33:2040 (abstr.).
2. Buchali A, Dinges S, Koswig S, et al. Virtuelle Simulation. Erste klinische Erfahrungen bei Patienten mit Prostatakarzinom. Strahlenther Onkol 1998; 174:88–91.
3. Deutschmann H, Kopp P, Kopp M, et al. Between virtual structures and reality. Proceedings of the 7th International Meeting on Progress in Radio-Oncology ICRO/ÖGRO 7, Salzburg, A. Bologna: Monduzzi, 2002.
4. Digital Imaging and Communications in Medicine (DICOM) Part 3. Information object definitions. Rosslyn: National Electrical Manufacturers Association, 2007 (*http://medical.nema.org*).
5. Elsayed H, Bölling T, Moustakis C, et al. Organ movements and dose exposures in teletherapy of prostate cancer using a rectal balloon. Strahlenther Onkol 2007;183:617–24.
6. Farmer FT, Fowler JF, Haggith JW. Megavoltage treatment planning and the use of xeroradiography. Br J Radiol 1963;36:426–35.
7. Guckenberger M, Meyer J, Wilbert J, et al. Precision of image-guided radiotherapy (IGRT) in six degrees of freedom and limitations in clinical practice. Strahlenther Onkol 2007;183:307–13.
8. Haidenberger A, Jobst M, Auer T, et al. Organbewegung der Prostata unter RT analysiert mittels Computertomographie – ein Problem der Strahlentherapie? Strahlenther Onkol 2006;182:Sondernr 1:195–6.
9. Hille A, Töws N, Schmidberger H, et al. A prospective three-dimensional analysis about the impact of differences in the clinical target volume in prostate cancer irradiation on normal-tissue exposure. A potential for increasing the benefit/risk ratio. Strahlenther Onkol 2005;181:789–95.
10. Hounsfield GN. Computerized transverse axial scanning (tomography). 1. Description of system. Br J Radiol 1973;46:1016–22.
11. Jeanneret-Sozzi W, Moeckli R, Valley JF, et al. The reasons for discrepancies in target volume delineation. Strahlenther Onkol 2006;182:450–7.
12. Kim TH, Kim DY, Cho KH, et al. Comparative analysis of the effects of belly board and bladder distension in postoperative radiotherapy of rectal cancer patients. Strahlenther Onkol 2005;181:601–5.
13. Milgram P, Takemura H, Utsumi A, et al. Augmented reality: a class of displays on the reality-virtuality continuum. SPIE vol 2351-34, Proceedings of Telemanipulator and Telepresence Technologies 1994:282–92.
14. Nishidai T, Nagata Y, Takahashi M, et al. CT simulator: a new 3-D planning and simulating system for radiotherapy. Part 2. Clinical application. Int J Radiat Oncol Biol Phys 1990;18:505–13.
15. Polat B, Wilbert J, Baier K, et al. Nonrigid patient setup errors in the head-and-neck region. Strahlenther Onkol 2007;183:506–11.
16. Schlegel W, Bortfeld T, Grosu A-L, eds. New technologies in radiation oncology. Berlin–Heidelberg–New York: Springer, 2006.
17. Sherouse GW, Novins K, Chaney EL. Computation of digitally reconstructed radiography for use in radiation treatment design. Int J Radiat Oncol Biol Phys 1990;18:651–8.
18. Smitsmans MHP, DeBois J, Sonke J-J, et al. Automatic prostate localization on cone-beam CT scans for high precision image-guided radiotherapy. Int J Rad Oncol Biol Phys 2005;63:975–84.
19. Treece GM, Prager RW, Gee AH, et al. Surface interpolation from sparse cross-sections using region correspondence. IEEE Trans Med Imaging 2000; 19:1106–14.
20. Trog D, Garbe S, Lutterbey G, et al. Volumetrische Veränderung der Mamma während der Radiotherapie. Ist vor Boostbestrahlung mit Elektronen eine Nachplanung erforderlich? Strahlenther Onkol 2005;181:255–9.
21. Valicenti RK. A prospective, randomized study addressing the need for physical simulation following virtual simulation. Int J Radiat Oncol Biol Phys 1997;39:1131–5.
22. Van Herk M, Remeijer P, Rasch C, et al. The probability of correct target dosage: dose-population histograms for deriving treatment margins in radiotherapy. Int J Radiat Oncol Biol Phys 2000;47:1121–35.
23. Wurstbauer K, Sedlmayer F, Kogelnik HD. Skin markings in external radiotherapy by temporary tattooing with henna: improvement of accuracy and increased patient comfort. Int J Rad Oncol Biol Phys 2001;50:179–81.

Address for Correspondence
Heinz Deutschmann
University Clinic for Radiotherapy and Radio-Oncology
Müllner Hauptstraße 48
5020 Salzburg
Austria
Phone (+43/662) 4482-3928, Fax -3903
e-mail: h.deutschmann@salk.at